Appl Phys B (2011) 104:487–493
DOI 10.1007/s00340-011-4648-3

Applied Physics B
Lasers and Optics

Nonlinear dynamics with higher-order modes in lithium niobate waveguide arrays

F. Setzpfandt · D.N. Neshev · A.A. Sukhorukov · R. Schiek · R. Ricken · Y. Min · Y.S. Kivshar · W. Sohler · F. Lederer · A. Tünnermann · T. Pertsch

Received: 31 March 2011 / Revised version: 5 June 2011 / Published online: 26 July 2011

Abstract We present theoretical and experimental studies on nonlinear beam propagation in lithium niobate waveguide arrays utilizing higher-order second harmonic bands. We find that the implementation of the higher-order second harmonic bands leads to a number of new effects. The combined interaction of two second harmonic bands with a propagating fundamental beam can lead to a complete inhibition of nonlinear effects or to the formation of discrete spatial solitons, depending only on the wavelength of the fundamental wave. Furthermore we analyze the properties of discrete solitons, allowing for linear coupling of the second harmonic. Here we predict and demonstrate experimentally a power dependent phase transition of the soliton topology.

F. Setzpfandt (✉) · A. Tünnermann · T. Pertsch
Institute of Applied Physics, Friedrich-Schiller-Universität Jena, Max-Wien-Platz 1, 07743 Jena, Germany
e-mail: f.setzpfandt@uni-jena.de

D.N. Neshev · A.A. Sukhorukov · Y.S. Kivshar
Nonlinear Physics Center, Research School of Physics and Engineering, Australian National University, Canberra, 0200 ACT, Australia

R. Schiek
University of Applied Sciences Regensburg, Prüfeninger Strasse 58, 93049 Regensburg, Germany

R. Ricken · Y. Min · W. Sohler
Applied Physics, Universität Paderborn, Warburger Strasse 100, 33095 Paderborn, Germany

F. Lederer
Institute for Condensed Matter Theory and Solid State Optics, Friedrich-Schiller-Universität Jena, Max-Wien-Platz 1, 07743 Jena, Germany

A. Tünnermann
Fraunhofer Institute for Applied Optics and Precision Engineering, Albert-Einstein-Strasse 7, 07745 Jena, Germany

1 Introduction

In the last years, discrete optics in waveguide arrays (WGAs) has been one of the most active fields in optical sciences [1–3]. The main reason for this lies in the unique properties of the periodic linear dispersion relation, or band structure, of a WGA. This band structure enables the ability to control the sign and strength of the diffraction of a linear beam [4, 5]. Since beam propagation in WGAs can be described similarly to the dynamics of electrons in atomic lattices, many effects predicted for electron motion in crystals have been observed in WGAs [6–8]. However, nonlinear WGAs have excited the most scientific interest, both for their importance in fundamental science [2, 9] and their potential applications [10–12].

The use of WGAs with quadratic nonlinearity further expands the possibilities of these kind of systems. Here optical fields of different frequencies are coupled by the nonlinear susceptibility. Specifically, a low-frequency fundamental wave (FW) field is coupled to its second harmonic (SH) with doubled frequency. This process may lead to an effective phase shift of the FW field which is mainly determined by the difference of the propagation constants of FW and SH [13–15]. Consequently, spatial focusing and defocusing [16] as well as spatial solitons [17–21] could be studied both theoretically and experimentally. However, in all experiments in WGAs up to now the nonlinear coupling of only the first bands of the FW and SH was exploited. As we will show here, many fundamental effects can only be observed if the FW band interacts with one or more higher-order SH bands. Coupling between fundamental and higher-order bands has

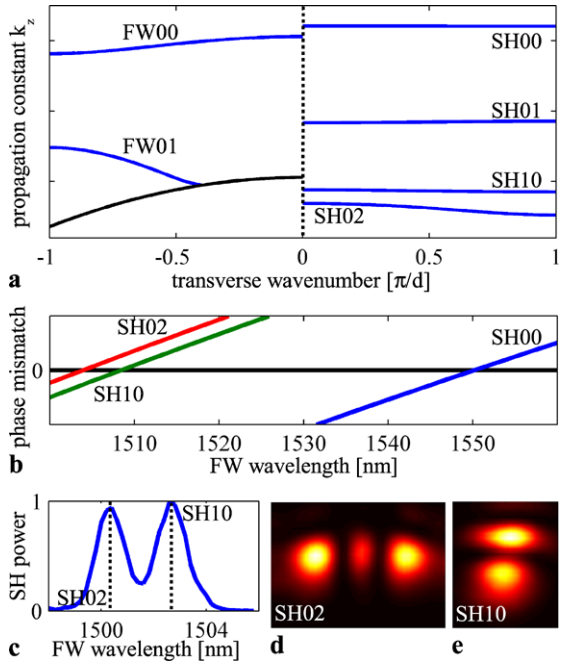

Fig. 1 (**a**) Scheme of the band structures of the FW (*left panel*) at 1500 nm and the SH (*right panel*) at 750 nm. The *black line* in the FW band structure shows the cut-off for guided modes. (**b**) Simulated phase mismatch between the FW00 and the SH00 (*blue*), SH10 (*green*), and SH02 (*red*) modes for $k_t = 0$. (**c**) Normalized SH output power for a broad beam at $k_t = 0$ as a function of the input FW wavelength. Maxima occur where the phasematching condition between a pair of FW and SH modes is fulfilled. (**d**, **e**) SH mode profiles at FW wavelengths of 1500.5 nm and 1502.6 nm, corresponding to the *dotted lines* in (**c**)

been used in nonlinear experiments in WGAs with third-order Kerr-type nonlinearity [22–25]. However, these systems are fundamentally different from WGAs with second-order nonlinearity considered here. In systems with Kerr nonlinearity, all observable effects stem from the bands that are selected upon excitation where the nature of the nonlinearity cannot be changed. In quadratic systems, only the FW component is excited directly. Here the utilized SH band as well as the effective cascading nonlinearity can be widely influenced by changing the FW wavelength.

The systems under consideration in this contribution are WGAs in lithium niobate made by titanium indiffusion [26]. The refractive index profile of these waveguides can be described analytically [27–29], and hence the band structure of the WGA can be calculated numerically. Figure 1(a) shows band structures calculated with a freely available software package based on the plane-wave expansion method [30]. We plot only the irreducible part of the first Brillouin zone for either wavelength. The left panel of Fig. 1(a) shows the bands for an FW wavelength of 1500 nm where the array supports only a fundamental mode over the complete range of transverse wavenumbers. For the corresponding SH wavelength of 750 nm, the array supports many guided modes, the first four bands are shown in the right panel of Fig. 1(a). The first FW band and the first four SH bands can be described in the coupled mode approximation since the spreading of the bands is small compared to the magnitude of the propagation constants and the bands do not overlap. The dependence of the propagation constant k_z^i on the transverse wavenumber k_t then is [5]:

$$k_z^i(\lambda, k_t) = k_0^i(\lambda) + 2c^i \cos(k_t d), \tag{1}$$

where the index i denotes the band and d is the period of the WGA. Here the band i is solely described by the two parameters coupling constant c^i and mean propagation constant k_0^i which corresponds to the propagation constant of the same mode in a single waveguide. For the SH00 band utilized in all nonlinear experiments up to now, the coupling constant c^{SH00} is negligible for all experimentally relevant cases. In this case the transverse dynamics of the SH is completely determined by the FW. In contrast, the coupling constants of the SH10 and especially the SH02 band can have the same magnitude as the FW00 coupling constant. As we will show later, this leads to new nonlinear propagation effects not observable before.

The strength of the nonlinear interaction between a pair of FW and SH bands is determined by the phase mismatch

$$\Delta k(\lambda, k_t) = 2k_z^{\mathrm{FW}}(\lambda, k_t) - k_z^{\mathrm{SH}}(\lambda, k_t) + 2\pi/\Lambda^{\mathrm{QPM}}, \tag{2}$$

where Λ^{QPM} accounts for the periodic poling of the nonlinear susceptibility of the WGA [31]. Since the mean propagation constants of the bands are dispersive, the phase mismatch for fixed transverse wavenumber can be tuned by changing the wavelength, as we show in Fig. 1(b). For a vanishing phase mismatch, the nonlinear interaction between the bands is the strongest, and the energy in the FW state is transferred to the corresponding SH state. The interaction strength is quickly decaying with increasing phase mismatch. The wavelength of phase mismatch between the FW00 and SH00 modes is far away from phasematching wavelengths to other SH modes. Hence an FW00 wave efficiently interacting with the SH00 band does not interact with other SH bands. In contrast to this, the wavelengths for phasematching between the FW00 and SH10 or SH02 modes are very close [see Fig. 1(b)]. Figure 1(c) shows the measured dependence of the SH power on the FW input wavelength for propagation of a broad input beam in a lithium niobate waveguide array. Figures 1(d,e) show the measured SH mode profiles at the wavelengths of maximum SH power, thus confirming that we nonlinearly couple to different higher-order SH bands. As was reported earlier for a single waveguide [32], both nonlinear processes can act simultaneously. Here we will show that the action of two different SH resonances can lead to new spatial effects during nonlinear propagation, namely the complete suppression of spatial beam reshaping. On the other hand, as we will show

here for the first time, with slightly different phase mismatch the formation of spatial solitons similar to [20] is possible were both participating SH modes contribute to the phase shifts necessary for soliton formation.

2 Nonlinear effects with two SH bands

Nonlinear beam propagation in a waveguide array with two SH bands may be described by the normalized coupled mode equations

$$
\begin{aligned}
&i\frac{dU_n^{\mathrm{FW}}}{dz} + c^{\mathrm{FW}}\left(U_{n+1}^{\mathrm{FW}} + U_{n-1}^{\mathrm{FW}}\right) \\
&\quad + \left(\gamma^{\mathrm{SH02}}U_n^{\mathrm{SH02}} + \gamma^{\mathrm{SH10}}\,U_n^{\mathrm{SH10}}\right)\left(U_n^{\mathrm{FW}}\right)^* = 0 \\
&i\frac{dU_n^{\mathrm{SH02}}}{dz} + c^{\mathrm{SH02}}\left(U_{n+1}^{\mathrm{SH02}} + U_{n-1}^{\mathrm{SH02}}\right) \\
&\quad - \Delta k^{\mathrm{SH02}}U_n^{\mathrm{SH02}} + \gamma^{\mathrm{SH02}}\left(U_n^{\mathrm{FW}}\right)^2 = 0 \\
&i\frac{dU_n^{\mathrm{SH10}}}{dz} + c^{\mathrm{SH10}}\left(U_{n+1}^{\mathrm{SH10}} + U_{n-1}^{\mathrm{SH10}}\right) \\
&\quad - \Delta k^{\mathrm{SH10}}U_n^{\mathrm{SH10}} + \gamma^{\mathrm{SH10}}\left(U_n^{\mathrm{FW}}\right)^2 = 0.
\end{aligned}
\tag{3}
$$

Here the U_n^j denote the amplitude of the mode field of the nth waveguide where the superscript $j = \{\mathrm{FW}, \mathrm{SH02}, \mathrm{SH10}\}$ indexes the field components. The c^j are the linear coupling constants. Δk^j and γ^j are the phase mismatches and nonlinear coupling strengths between the FW mode and the SH mode labeled by j.

Since the two SH modes are orthogonal to each other, they do not directly interact linearly. However, they both interact nonlinearly with the FW field. It was shown for interactions of one pair of FW and SH modes [14] that for nonzero phase mismatch the cascaded FW–SH interaction leads to effective nonlinearities comparable to Kerr nonlinearities. For positive phase mismatch, these cascaded nonlinearity is focusing, whereas it is defocussing for negative phase mismatch. In the system considered here, two of such interactions act on the FW [see Fig. 1(c)]. For positive or negative phase mismatch of both nonlinear interactions, the nature of the cascaded nonlinearity will not change. However, for the case of different signs of the two mismatches, both nonlinear processes will compete, and the overall nonlinear strength will be greatly diminished [33].

To show these effects experimentally, we investigate the propagation of a wide Gaussian beam in a lithium niobate WGA. The used sample consists of 101 waveguides with a period of $d = 15$ µm and a phasematching period of $\Lambda^{\mathrm{QPM}} = 16.803$ µm. The linear coupling constants are $c^{\mathrm{FW}} \approx 80/\mathrm{m}$, $c^{\mathrm{SH02}} \approx 80/\mathrm{m}$, and $c^{\mathrm{SH10}} \approx 16/\mathrm{m}$ for FW input wavelengths of 1500 nm and the corresponding SH wavelength of 750 nm. To obtain the high necessary peak powers, we use 5.2-ps pulses generated by a noncollinear optical parametric amplifier [34], which is seeded by a tuneable cw diode laser. With the help of a cylindrical telescope, the laser beam is shaped to an ellipse with a horizontal (vertical) width of ≈60 µm (3 µm) and coupled into the sample. To characterize the array output, we measure the FW and SH output powers and record the spatial profiles of both components with an InGaAs and a CCD camera, respectively. As a comprehensive number to describe nonlinear spatial effects, we calculate the width of the FW part of the beam as the second moment of the measured FW output intensity distribution.

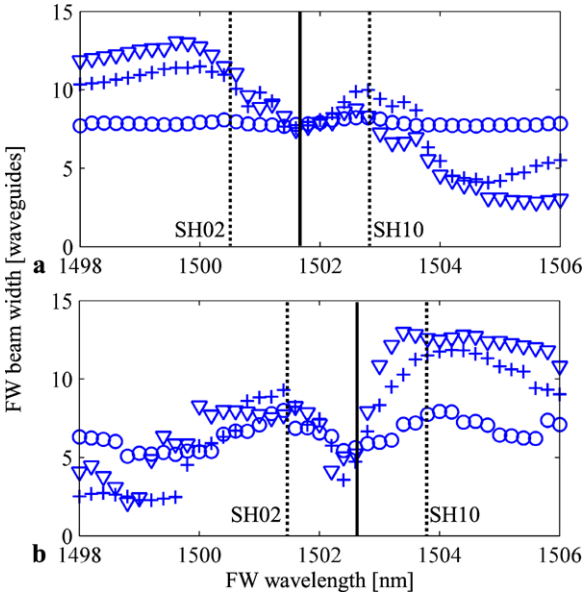

Fig. 2 Width of the output FW intensity distribution in dependence on the wavelength for (**a**) unstaggered and (**b**) staggered excitation. The curves are plotted for input powers of 0.05 kW (*circles*), 0.6 kW (*crosses*), and 1.3 kW (*triangles*), respectively. The *dotted lines* mark the phase-matching wavelengths, whereas the solid lines mark the wavelengths of nonlinearity inhibition

Figure 2(a) shows the results for normal incidence of the coupled FW beam. Here FW states in the center of the periodic dispersion relation are excited, which have the same phase in all waveguides (unstaggered excitation). For the lowest measured power, the beam width does not depend on the input wavelength. Here almost no nonlinear effects take place. For higher input power, we observe a strong focusing (defocusing) for wavelengths above (below) both phase-matching resonances. This is due to the mismatch induced cascaded nonlinearity. However, for the wavelength between the phase-matching resonances, the FW beam width stays the same for all powers. Here the different signs of the mismatches from both resonances lead to a complete cancellation of spatial nonlinear effects [33].

The same measurement is conducted for an excitation at the edge of the Brillouin zone. This is achieved by tilting the input FW beam until the phase difference between adjacent

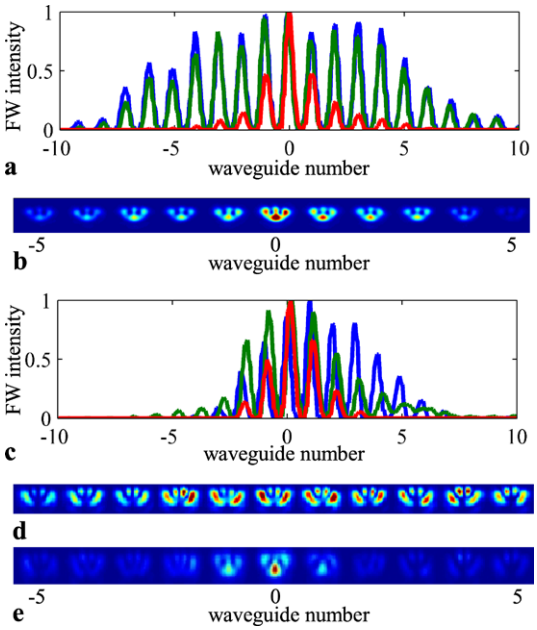

Fig. 3 (**a**) Normalized FW output intensity profiles for normal incidence for 0.05 kW (*blue*) and 1.3 kW (*red*) input peak power at a wavelength of 1506 nm showing soliton formation. The output intensity at the wavelength of nonlinearity compensation 1501.6 nm is also shown for 1.3 kW (*green*). (**b**) SH mode profiles for an FW wavelength of 1506 nm for 1.3 kW input power. (**c**) Same as (**a**) for tilted incidence at the edge of the Brillouin zone. Here the wavelength for soliton formation is 1498 nm, and the compensation wavelength is 1502.6 nm. (**d**) SH mode profiles at tilted FW incidence for low input power. (**e**) SH soliton profile for tilted incidence and an input power of 1.3 kW

waveguides is π (staggered excitation). The measured beam widths are presented in Fig. 2(b). Qualitatively, the image is reversed with respect to Fig. 2(a). This is due to the negative curvature of the FW band at the band edge $k_t^{\mathrm{FW}} = \pi$. Here the linear beam undergoes anomalous diffraction [5]. Hence the focusing cascading nonlinearity present at long wavelengths broadens the beam, while the short wavelength defocusing nonlinearity is narrowing the beam. However, the inhibition of all spatial nonlinear effects between the phase-matching wavelengths is again observed. The deviations in the beam width at the inhibition wavelength can be attributed to other excited modes as we will show in the following by analyzing output profiles of FW and SH.

Figure 3 shows typical intensity profiles of the characteristic spatial output of the waveguide array for the different nonlinear scenarios described above. Specifically, in Fig. 3(a) the FW profiles corresponding to low-power propagation, nonlinear competition, and soliton formation are plotted for unstaggered excitation. As expected from the width data given in Fig. 2(a), the profiles for the linear propagation (blue) at a wavelength of 1506 nm and nonlinearity inhibition (green) at 1501.6 nm are equal. For a wavelength of 1506 nm, where Fig. 2(a) indicated nonlinear focusing of the FW beam for 1.3-kW input peak power, the measured profile (red) corresponds to a discrete quadratic soliton. In contrast to Ref. [20], the SH part of these solitons consists of contributions from the SH02 and SH10 bands. This was confirmed by a measurement of the SH mode profiles at the array output, presented in Fig. 3(b). Clearly, the measured mode profiles are an interference of the mode profiles shown in Fig. 1(d,e). This evidences that we indeed for the first time detected discrete quadratic solitons with higher-order SH modes. The same measurements were performed for staggered incidence. Figure 3(c) shows again the FW output profiles for linear propagation (blue) and soliton formation (red) at 1498.6 nm as well as for nonlinearity inhibition (green) at 1502.5 nm. Here, the output profile for the nonlinearity inhibition wavelength is narrower than the low-power FW output pattern. However, the spatial reshaping is much less pronounced than in the case of soliton formation. The deviations from total inhibition of spatial reshaping are due to additional modes contributing to the nonlinear dynamics. For staggered propagation at transverse wavenumbers of $\pm\pi$, the array supports higher order propagating modes also for the FW wavelength [see Fig. 1(a)], hence also the FW01 band is weakly excited. In this case, nonlinear coupling between both FW modes and SH modes other than SH10 and SH02 takes place. These additional FW-SH interactions lead to spatial nonlinear effects which cannot be fully canceled. In Fig. 3(d) the SH output profile at low power for the soliton wavelength of 1498.6 nm is plotted. The dominating SH mode excited here is the SH11 mode. Additional simulations also predict phase-matching to the SH03 mode for wavelengths close to the competition wavelength. However, for higher powers and especially for soliton formation, the modes SH02 and SH10 play a dominating role. This is evidenced by Fig. 3(e), which shows the SH mode profile of the soliton plotted in Fig. 3(c). Clearly the center of the soliton is composed of the SH02 and SH10 modes, whereas the mode profiles in the wings belong to the spurious SH modes.

3 Soliton phase transition

In Sect. 2 we experimentally verified the existence of discrete quadratic solitons with higher-order SH modes. Here we will show that the properties of these higher-order bands, namely the nonvanishing linear coupling, lead to properties of the solitons different from these with first-order SH modes [35]. Solitons were shown to exist in regions were both nonlinear interactions have the same sign. Here the nonlinear dynamics of the systems is dominated by the phase-matching resonance with the smaller mismatch. To gain a physical insight into the basic properties of these solitons, we first analyze the stationary solutions of a simplified form of coupled mode equations, (3), dropping one of the SH modes. We further assume that the remaining components have the same linear coupling strength, which in the

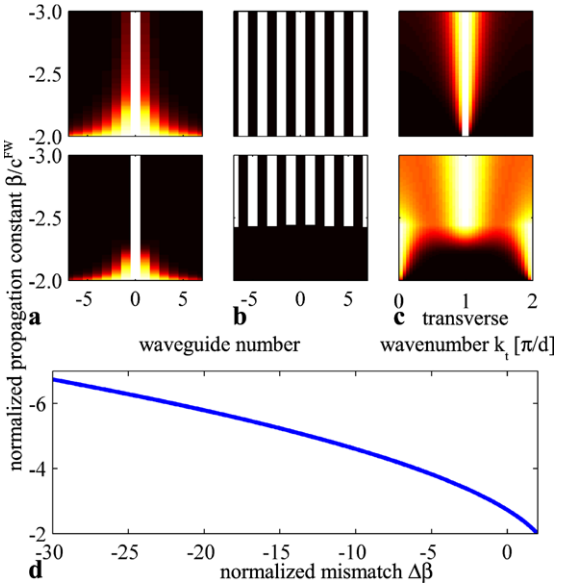

Fig. 4 (**a**) Absolute values of the mode amplitudes, (**b**) phases (*black* corresponds to 0, and *white* to π), and (**c**) absolute values of the spatial Fourier spectra for the soliton family at $\Delta\beta = 1$. The *upper row* show numerical results for the FW, and the *lower row* for the SH part of the solution. (**d**) Threshold propagation constant for the topology transition observed in the SH part of (**b**,**c**) in dependence on the mismatch

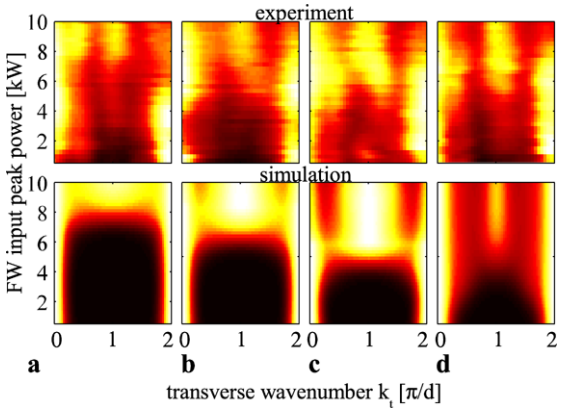

Fig. 5 Power dependence of the SH spatial output spectrum for an FW wavelength (normalized mismatch) of (**a**) 1498 nm (−25.5), (**b**) 1499 nm (−17.1), (**c**) 1500 nm (−7.7), and (**d**) 1501 nm (0.9). The *upper row* shows experimental results, and the *lower row* results of simulations of the time-dependent coupled mode equations

experiment is fulfilled for the SH02 band. Specifically, we will focus on solitons with staggered FW part. Stationary solutions of the simplified coupled mode equations have the form

$$U_n^{\mathrm{FW}}(z) = U_n^{\mathrm{FW}}(z=0)\exp(i\beta z),$$
$$U_n^{\mathrm{SH02}}(z) = U_n^{\mathrm{SH02}}(z=0)\exp(i2\beta z). \tag{4}$$

Here the real parameter β describes the propagation constants of both FW and SH due to nonlinear synchronization. We substitute these equations into the coupled mode equations and obtain a nonlinear system of equations for the real amplitudes of the FW and SH parts of the stationary solutions. This system is solved numerically in dependence on the mismatch for propagation constants below the linear bands of FW and SH to obtain solitons with staggered FW part [18, 35]. Results for a normalized mismatch of $\Delta\beta = \left(\Delta k^{\mathrm{SH02}} + 2c_{\mathrm{FW}}\right)/c_{\mathrm{FW}} = 1$ are plotted in Fig. 4(a–c). In Fig. 4(a) we plot the amplitudes of the FW and SH as functions of the propagation constant. With increasing magnitude of the propagation constant, the solutions are getting narrower and simultaneously increase their energy. The most important features are found in the phases of the solutions, plotted in Fig. 4(b). The phases of the FW are staggered; however the phase profile of the SH component abruptly changes from unstaggered at small negative propagation constants to staggered for increasing magnitude of the propagation constant. In the staggered domain, the SH dynamics is completely controlled by the wide FW part of the soliton via nonlinear coupling, and the phase-matching conditions force the SH to be unstaggered. However, when the solitons are getting narrower, the SH dynamics is mostly governed by the linear SH coupling, and hence the SH profile becomes staggered [35]. An experimentally accessible signature of this phase transition is the SH intensity distribution in the spatial spectrum, shown in Fig. 4(c). For unstaggered SH, the intensity is concentrated in the center of the Brillouin zone at $k_t = 0, 2\,\pi/d$. When the phase transition takes place, the maximum of the SH intensity switches to the boundaries of the SH Brillouin zone at $k_t = \pi/d$. The critical soliton propagation constant where the phase transition occurs can be calculated analytically by analyzing the tails of the stationary solutions [35]. The result, plotted in Fig. 4(d), shows that the phase transition exists for a large number of input conditions and the magnitude of its threshold propagation constant is monotonically increasing with increasing magnitude of the mismatch. The analytical considerations also show that the critical propagation constant for the phase transition goes to infinity if the linear SH coupling approaches zero. Hence the appearance of the phase transition is unambiguously linked to the coupling of the SH band.

To prove the existence of the phase transition experimentally, we launch a staggered FW beam in the array. The spatial spectrum of the SH is obtained by employing an additional lens and a CCD camera. The experimental parameters are similar to the ones described in Sect. 2. Although we experimentally show the existence of staggered discrete quadratic solitons for these parameters, the stable excitation of the narrow solitons exhibiting the phase transition is not possible with FW only input [36]. Nevertheless, as the upper row of Fig. 5 shows, the features of the phase transition could be experimentally reproduced for wavelengths corresponding to normalized mismatches from $\Delta\beta = -25$

to $\Delta\beta = 1$. For low powers, the SH intensity is exclusively concentrated at transverse wavenumber of $k_t = 0, 2\pi/d$. If the power is increased, which corresponds to increased magnitude of the propagation constants of the stationary solutions, the staggered SH is generated also at the edge of the Brillouin zone at $k_t = \pi/d$. In accordance with the predicted dependency of the critical soliton propagation constant on the mismatch [see Fig. 4(d)], the experimental phase transition power grows with larger magnitude of the mismatch. In contrast to the results obtained for the stationary solutions, the transition from unstaggered to staggered is not complete in the experiments, leading to nonzero intensities at $k_t = 0, 2\,\pi/d$ for all input powers. This is due to the use of short laser pulses in the experiments which lead to more complex spatio-temporal dynamics not accounted for in the stationary analysis. To confirm this, we conducted simulations of the time-dependent coupled mode equations where we include group velocity mismatch, pulse dispersion [20, 37], and the interaction with the SH10 mode. The results of this simulations are shown in the lower row of Fig. 5 and agree very well with the measured data. Hence we proved experimentally that the SH phase transition is not only a feature of discrete quadratic solitons but a generic phenomenon of nonlinear propagation with linearly coupled SH waves.

4 Conclusions

We have analyzed nonlinear light propagation in lithium niobate waveguide arrays where the SH part of the propagating fields is composed from higher-order SH bands. We have shown experimentally that in such a setup the system shows propagation effects which are distinct from the results of earlier studies where the first-order SH band has been used. We have identified two settings which cannot be obtained while using the first-order SH band. First, the close spacing of the higher-order bands allows us to study interactions of an FW beam with two or more SH components. For wavelengths between the phase-matching wavelengths to the two participating SH bands, this leads to weakening or complete inhibition of spatial nonlinear beam reshaping [33]. This effect may be valuable in high-power applications were nonlinear effects need to be suppressed. For wavelengths above or below the phase-matching wavelengths, we have shown that discrete spatial solitons can be excited with both SH bands contributing to the effective Kerr-type nonlinear response. Theoretically we found that, due to the linear coupling of the SH bands, these solitons exhibit a new localization-controlled phase transition of the topology of the SH part. This phase transition is generic in nonlinear systems with coupled SH, and we have been able to verify it experimentally [35]. We believe that this transition can occur in other systems described with coupled mode equations similar to (3). In optics it can be used for generating specific phase structures.

Acknowledgements The authors acknowledge support from the Deutsche Forschungsgemeinschaft (Research Unit 532 "Nonlinear spatial-temporal dynamics in dissipative and discrete optical systems"), the Federal Ministry of Education and Research (Innoregio-ZIK), the Go8-DAAD (Australia-Germany Joint Research Cooperation Scheme), and the Australian Research Council.

References

1. D.N. Christodoulides, F. Lederer, Y. Silberberg, Nature **424**, 817 (2003)
2. F. Lederer, G.I. Stegeman, D.N. Christodoulides, G. Assanto, M. Segev, Y. Silberberg, Phys. Rep. **463**, 1 (2008)
3. C. Denz, S. Flach, Y.S. Kivshar (eds.), *Nonlinearities in Periodic Structures and Metamaterials* (Springer, Berlin, 2010)
4. H.S. Eisenberg, Y. Silberberg, R. Morandotti, J.S. Aitchison, Phys. Rev. Lett. **85**, 1863 (2000)
5. T. Pertsch, T. Zentgraf, U. Peschel, A. Bräuer, F. Lederer, Phys. Rev. Lett. **88**, 093901 (2002)
6. H. Trompeter, T. Pertsch, F. Lederer, D. Michaelis, U. Streppel, A. Bräuer, U. Peschel, Phys. Rev. Lett. **96**, 023901 (2006)
7. H. Trompeter, W. Krolikowski, D.N. Neshev, A.S. Desyatnikov, A.A. Sukhorukov, Y.S. Kivshar, T. Pertsch, U. Peschel, F. Lederer, Phys. Rev. Lett. **96**, 053903 (2006)
8. A. Szameit, I.L. Garanovich, M. Heinrich, A.A. Sukhorukov, F. Dreisow, T. Pertsch, S. Nolte, A. Tünnermann, Y.S. Kivshar, Nat. Phys. **5**, 271 (2009)
9. H.S. Eisenberg, Y. Silberberg, R. Morandotti, A.R. Boyd, J.S. Aitchison, Phys. Rev. Lett. **81**, 3383 (1998)
10. A.B. Aceves, C.D. Angelis, S. Trillo, S. Wabnitz, Opt. Lett. **19**, 332 (1994)
11. O. Bang, P.D. Miller, Opt. Lett. **21**, 1105 (1996)
12. R.A. Vicencio, M.I. Molina, Y.S. Kivshar, Opt. Lett. **28**, 1942 (2003)
13. G.I. Stegeman, M. Sheik-Bahae, E.V. Stryland, G. Assanto, Opt. Lett. **18**, 13 (1993)
14. A. Kobyakov, F. Lederer, Phys. Rev. A **54**, 3455 (1996)
15. R. Schiek, Y. Baek, G.I. Stegeman, J. Opt. Soc. Am. B **15**, 2255 (1998)
16. R. DeSalvo, D.J. Hagan, M. Sheik-Bahae, G. Stegeman, E.W.V. Stryland, H. Vanherzeele, Opt. Lett. **17**, 28 (1992)
17. O. Bang, P.L. Christiansen, C.B. Clausen, Phys. Rev. E **56**, 7257 (1997)
18. T. Peschel, U. Peschel, F. Lederer, Phys. Rev. E **57**, 1127 (1998)
19. S. Darmanyan, A. Kobyakov, F. Lederer, Phys. Rev. E **57**, 2344 (1998)
20. R. Iwanow, R. Schiek, G.I. Stegeman, T. Pertsch, F. Lederer, Y. Min, W. Sohler, Phys. Rev. Lett. **93**, 113902 (2004)
21. A.A. Sukhorukov, Y.S. Kivshar, O. Bang, C.M. Soukoulis, Phys. Rev. E **63**, 016615 (2000)
22. D. Mandelik, H.S. Eisenberg, Y. Silberberg, R. Morandotti, J.S. Aitchison, Phys. Rev. Lett. **90**, 053902 (2003)
23. D. Mandelik, H.S. Eisenberg, Y. Silberberg, R. Morandotti, J.S. Aitchison, Phys. Rev. Lett. **90**, 253902 (2003)
24. C. Rosberg, B. Hanna, D. Neshev, A. Sukhorukov, W. Krolikowski, Y. Kivshar, Opt. Express **13**, 5369 (2005)
25. A. Fratalocchi, G. Assanto, K.A. Brzdakiewicz, M.A. Karpierz, Opt. Lett. **30**, 174 (2005)
26. W. Sohler, H. Hu, R. Ricken, V. Quiring, C. Vannahme, H. Herrmann, D. Büchter, S. Reza, W. Grundkötter, S. Orlov, H. Suche, R. Nouroozi, Y. Min, Opt. Photonics News **19**, 24 (2008)

27. W.K. Burns, P.H. Klein, E.J. West, L. Plew, J. Appl. Phys. **50**, 6175 (1979)
28. G.J. Edwards, M. Lawrence, Electronics **16**, 373 (1984)
29. E. Strake, G. Bava, I. Montrosset, J. Lightwave Technol. **6**, 1126 (1988)
30. S. Johnson, J. Joannopoulos, Opt. Express **8**, 173 (2001)
31. M. Houe, P.D. Townsend, J. Phys. D, Appl. Phys. **28**, 1747 (1995)
32. C.G. Trevino-Palacios, G.I. Stegeman, M.P.D. Micheli, P. Baldi, S. Nouh, D.B. Ostrowsky, D. Delacourt, M. Papuchon, Appl. Phys. Lett. **67**, 170 (1995)
33. F. Setzpfandt, D.N. Neshev, R. Schiek, F. Lederer, A. Tünnermann, T. Pertsch, Opt. Lett. **34**, 3589 (2009)
34. M. Breuer, C. Homann, E. Riedle, *Noncollinear Optical Parametric Amplification of Cw Light, Continua and Vacuum Fluctuations*. Springer Series in Chemical Physics, vol. 92 (Springer, Berlin, 2009), pp. 771–773
35. F. Setzpfandt, A.A. Sukhorukov, D.N. Neshev, R. Schiek, Y.S. Kivshar, T. Pertsch, Phys. Rev. Lett. **105**, 233905 (2010)
36. R. Iwanow, G.I. Stegeman, R. Schiek, T. Pertsch, F. Lederer, Y. Min, W. Sohler, Opt. Lett. **30**, 1033 (2005)
37. C.R. Menyuk, R. Schiek, L. Torner, J. Opt. Soc. Am. B **11**, 2434 (1994)